






Saharan Dust Effects on North Atlantic Sea-Surface Skin Temperatures

Bingkun Luo¹ , Peter J. Minnett¹ , Paquita Zuidema¹ , Nicholas R. Nalli² , and Santha Akella³ ¹Rosenstiel School of Marine and Atmospheric Science, University of Miami, Miami, FL, USA, ²TMSG, Inc. at National Oceanic and Atmospheric Administration (NOAA) NESDIS/STAR, College Park, MD, USA, ³NASA Goddard Space Flight Center, Global Modeling and Assimilation Office (GMAO), Greenbelt, MD, USA

Key Points:

- Using independent shipboard measurements and MERRA-2 reanalysis in the tropical Atlantic Ocean
- The dust outbreaks can decrease the surface shortwave radiation up to 190 W/m² and increase the surface longwave radiation by up to 14W/m²
- Skin sea-surface temperature response to the abnormal surface radiative fluxes can range from a net cooling to a tiny warming: −0.24 to 0.06K

Correspondence to:

B. Luo,
LBK@rsmas.miami.edu

Citation:

Luo, B., Minnett, P. J., Zuidema, P., Nalli, N. R., & Akella, S. (2021). Saharan dust effects on North Atlantic sea-surface skin temperatures. *Journal of Geophysical Research: Oceans*, 126, e2021JC017282. <https://doi.org/10.1029/2021JC017282>Received 12 FEB 2021
Accepted 30 MAR 2021

Abstract Saharan dust outbreaks frequently propagate westward over the Atlantic Ocean; accurate quantification of the dust aerosol scattering and absorption effect on the surface radiative fluxes (SRF) is fundamental to understanding critical climate feedbacks. By exploiting large sets of measurements from many ship campaigns in conjunction with reanalysis products, this study characterizes the sensitivity of the SRF and skin Sea-Surface Temperature (SST_{skin}) to the Saharan dust aerosols using models of the atmospheric radiative transfer and thermal skin effect. Saharan dust outbreaks can decrease the surface shortwave radiation up to 190 W/m², and an analysis of the corresponding SST_{skin} changes using a thermal skin model suggests dust-induced cooling effects as large as −0.24 K during daytime and a warming effect of up to 0.06 K during daytime and nighttime respectively. Greater physical insight into the radiative transfer through an aerosol-burdened atmosphere will substantially improve the predictive capabilities of weather and climate studies on a regional basis.

Plain Language Summary Accurate independent shipboard measurements in the tropical Atlantic Ocean area provide an independent representation of the atmosphere and ocean that can be used to investigate the influence of the dust aerosols on skin Sea-Surface Temperature (SST_{skin}) variability. The NASA MERRA-2 reanalysis fields augment the radiosonde data to characterize the vertical dust aerosol profiles at the times and places where radiosondes were launched, and to provide inputs for radiative transfer calculations. This study includes the RRTMG-simulated surface shortwave and net longwave downwelling radiative changes due to dust and calculates the corresponding thermal skin layer temperature changes.

1. Introduction and Background

Skin sea-surface temperatures (SST_{skin}) provide a key indicator of the air-sea exchanges at the ocean surface as well as the acquisition, storage, transport, and release of heat. The majority of the incoming solar radiation is absorbed in the upper ocean; most of the resulting heat gain is released to the lower atmosphere, helping to drive weather and climate. The Surface Radiative Fluxes (SRF) are influenced by the atmospheric state (Kato et al., 2020; Wild et al., 2013; Yamada & Hayasaka, 2016). The Saharan Air Layer (SAL) is a particular atmospheric anomaly that frequently occurs at large scales in the tropical North Atlantic Ocean and has consequences on the surface radiation budget (Evan et al., 2009; Yu et al., 2006), on the development of severe storms (Zhang et al., 2007), and on the accuracy of satellite-derived SST_{skin} (Luo et al., 2019; Merchant et al., 2006). The SAL is a typically warm and dry air layer that can reside up to 5 km in altitude, and is often accompanied by dust aerosols (Carlson & Prospero, 1972; Dunion & Velden, 2004; Nalli et al., 2011; Wu, 2007).

The dust aerosol particles are found with diameters exceeding 10 μm even after long-range transport (e.g., Kramer et al., 2020), allowing them to absorb, scatter and emit infrared radiation (Kok et al., 2017). Indeed, many studies have made efforts to quantify dust direct radiative effects (e.g., Doherty & Evan 2014; Hansell et al., 2010; Song et al., 2018; Thorsen et al., 2020; Zuidema et al., 2008). The ocean gains most of its heat from the absorption in the upper-layer of shortwave radiation during the daytime and loses the heat through the ocean surface nearly all the time through infrared emission and turbulent fluxes. Thus, the anomalies in SRF due to aerosol radiative effects can impact the sea-surface temperatures (SSTs) and

upper ocean heat content, especially the diurnal warming layer, also referred to as the diurnal thermocline (Gentemann et al., 2009). Numerous studies have attempted to analyze the impact of dust aerosols on SST: Foltz and McPhaden (2008) used combinations of satellite-derived aerosol optical depth (AOD) and in situ measurements obtained from the PIRATA mooring data to investigate the relations between SST anomalies and AOD anomalies. They found that the dust outflows were always associated with a reduction in solar radiation, and about 35% of the SST variability was related to dust outbreaks; other SST cool anomalies were due to wind stress. Evan et al. (2009) used 26 years of satellite-derived SST and AOD retrievals to model the response of the temperature of the mixed layer to changes in dust AOD, which were shown to decrease over the period studied, with aerosols accounting for 69% of the upward trend in the mixed-layer temperature. Martínez Avellaneda et al., (2010) analyzed the MODerate resolution Imaging Spectroradiometer (MODIS) derived AOD and TRMM Microwave Imager (TMI) derived SST with a physical model to estimate the Saharan dust impact on North Atlantic SST. The dust associated SST shortwave cooling was found to range from 0.2 to 0.4 K. About 30% of the climatological SST variance could be explained by the dust cooling scheme at low wind speed conditions. Lau and Kim (2007) estimated the solar radiation attenuation by dust aerosols which could explain 30%–40% of the SST cooling patterns, and that the cooling rate depends on the mixed layer depth. Evan et al. (2011) presented the effects of the dust aerosols on air-sea interface variability with satellite datasets; they found the dust-forced SST anomalies were related to the Atlantic Meridional Mode (Vimont & Kossin, 2007).

However, all of the above studies were performed using satellite datasets and models. Compared to the Top of Atmosphere (TOA) radiation being directly monitored by satellites, estimates of the perturbations of the surface radiative budget caused by dust aerosols are difficult to derive from satellite data due to the additional complexities in the retrieval process, and imperfect understanding of the atmospheric radiative effects (Kato et al., 2013). The determination of aerosol radiative forcing at the sea surface can also be undermined by the limited availability of direct measurements. Furthermore, estimating the correct dust effect on SST in different geographical locations requires a sufficiently large in situ data set and accurate models of the thermal skin effect and diurnal heating. None of the aforementioned studies are based on a long-term analysis of in situ data. The lack of in situ measurements at the sea surface has hampered studies of the effects of dust aerosol SRF on SST over the tropical North Atlantic Ocean.

This study uses measurements from a suite of AERosol and Ocean Science Expedition (AEROSE) campaigns that have provided appropriate atmospheric and oceanic datasets (Nalli et al., 2011), augmented with reanalysis dust aerosol profiles throughout the tropical North Atlantic Ocean, with the objective of a better understanding of the aerosol radiative forcing, both infrared and shortwave, on the SST_{skin} . Since the SRF variations are modulated by radiative feedback processes, a critical tool is provided by radiative transfer models, which allow the isolation of different internal and external factors and an examination of their relationships with each other. In this study, the shortwave and longwave radiative fluxes are calculated with the Rapid Radiative Transfer Model for General Circulation Models Applications (RRTMG; Iacono et al. (2008)). The downwelling radiative effects of dust also have an impact on the SST_{skin} . A widely used skin layer and diurnal model that includes convection and insolation absorption effects was developed by Fairall et al. (1996a) and further refined by Zeng and Beljaars (2005), Takaya et al. (2010), and Gentemann et al. (2009). In our study, the dust radiative effects on SST_{skin} are simulated by models of the thermal skin used in the NASA Global Modeling and Assimilation Office (GMAO) Weather Analysis and Prediction System (https://gmao.gsfc.nasa.gov/weather_prediction/), MERRA-2 (Modern-Era Retrospective analysis for Research and Applications, version 2; Randles et al. (2017)); MERRA-2 reanalysis used daily $1/4$ deg Reynolds SST (Reynolds & Smith, 1994) as foundation SST before Apr 2006, thereafter the daily OSTIA product (Donlon et al., 2012) was used, see (Akella et al., 2017) for details and the aerosol information is also from the NASA GMAO MERRA-2 (Modern-Era Retrospective analysis for Research and Applications, version 2; Randles et al. (2017)) atmospheric reanalysis, see Section 2.2 for further details. The extensive datasets from AEROSE campaigns can be used as valuable inputs for the RRTMG model, as well as examining the dust radiative effects on SST_{skin} . Greater physical insight into the downwelling radiative effect of Saharan dust aerosols on SST_{skin} will substantially improve the predictive capabilities of weather and climate models in the Atlantic Ocean area.

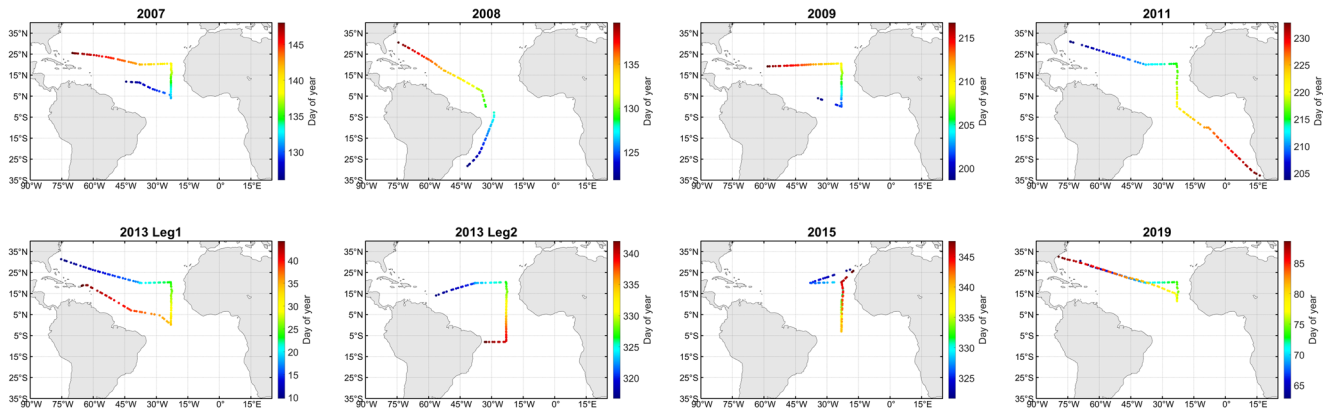


Figure 1. Cruise tracks of each AEROSE campaign, the points indicate the radiosonde deployment locations. The colors indicate day of the year.

2. Data and Study Fields

2.1. AEROSE in situ Data

In situ measured data from research ships collected during a series of AEROSE campaigns (Morris et al., 2006; Nalli et al., 2011) onboard the NOAA Ship *Ronald H. Brown* and the R/V *Alliance* and remotely derived datasets are used to assess the Saharan dust effects on SST_{skin} . AEROSE was a sequence of Atlantic field campaigns from 2004 to the present, aiming to take accurate oceanic and atmospheric measurements of the tropical Atlantic Ocean under Saharan dust outbreaks (Nalli et al., 2011); Figure 1 shows the AEROSE ship tracks of each year, where the colors indicate day of the year. Table 1 summarizes the cruise starting and ending dates as well as the number of radiosondes deployed in each of the AEROSE cruises that were used in this study. A total of 751 radiosonde profiles over a span of 231 days were used. The measurements made during these campaigns provided data that were required as inputs for radiative transfer models and models of the thermal skin and diurnal heating.

One of the key instruments is the Marine-Atmospheric Emitted Radiance Interferometer (M-AERI), which is a Fourier-transform infrared spectro-radiometer which measures spectra in the wavenumber range of $500\text{--}3,000\text{ cm}^{-1}$ ($3.3\text{--}20\text{ }\mu\text{m}$) (Minnett et al., 2001). An M-AERI was mounted on the ships for each AEROSE cruise. Highly accurate SST_{skin} can be retrieved from M-AERI measurements. An error budget of the SST_{skin} derived from the M-AERI measurements gives a root mean square accuracy of about 40 mK. The M-AERI infrared spectra can also be used to retrieve the lower troposphere temperature and humidity profiles from the measurements of CO_2 emission spectra (Szczo drak et al., 2007). M-AERI SST_{skin} retrievals have been widely used to validate satellite-derived SST_{skin} (Kearns et al., 2000; Kilpatrick et al., 2015;

Luo & Minnett, 2021; Luo et al., 2019, 2020a, 2021; Minnett et al., 2020a], and reanalysis model output SST_{skin} , such as those from MERRA-2 (Luo et al., 2020b) and ERA-5 (Luo & Minnett, 2020).

During the AEROSE cruises, two to four radiosondes were deployed each day to measure the vertical air temperature and water vapor profiles. Figure 2, rows 1–2, show the relative humidity and rows 3–4 show the air temperature along each of the AEROSE tracks. These intensive observations provide us with the opportunity to quantify dust aerosol radiative forcing on the SRF and SST_{skin} ; the dense network of observations will benefit the radiative transfer model simulations.

2.2. MERRA-2 Data

This study uses data from the NASA MERRA-2 (Gelaro et al., 2017), which contains geolocated dust aerosol mixing ratio at 72 standard pressure levels with one or three hours temporal resolution which is extraordinarily

Table 1
Details of the AEROSE Cruises

Cruises	Number of radiosondes	Start	End	Days of data
2007	96	2007-05-07	2007-05-28	22
2008	74	2008-04-29	2008-05-19	21
2009	78	2009-07-11	2009-08-11	31
2011	102	2011-07-21	2011-08-20	31
2013 Leg 1	111	2013-01-09	2013-02-13	36
2013 Leg 2	97	2013-11-11	2013-12-08	28
2015	92	2015-11-17	2015-12-14	28
2019	101	2019-02-24	2019-03-29	34
Total	751	2007-05-07	2019-03-29	231

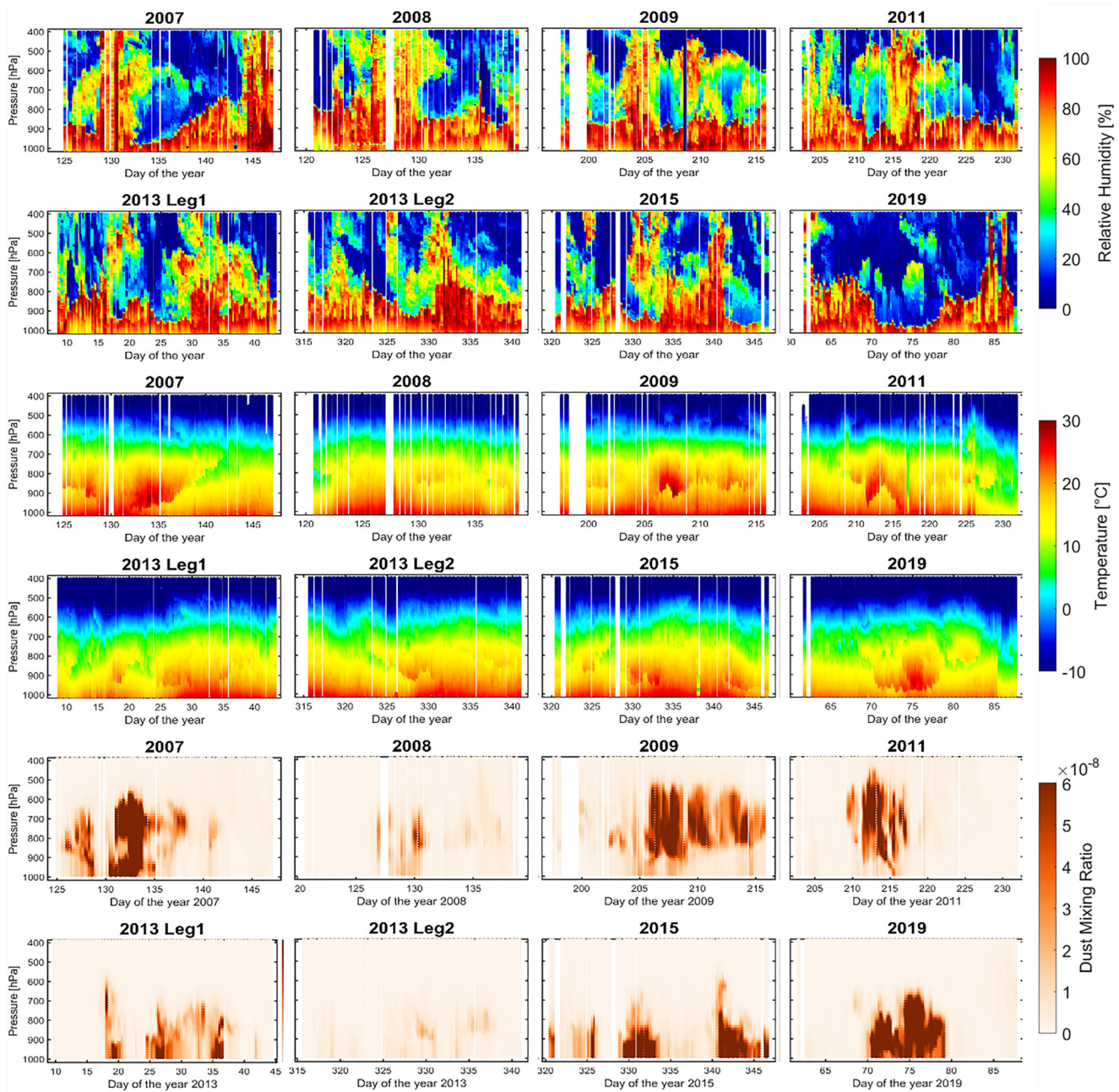


Figure 2. Rows 1–2: Relative humidity measured by radiosondes launched from the ships, the dust introduced dry layers are visible on some days. Rows 3–4: Air temperatures measured by radiosondes (Luo et al., 2020b). Rows 5–6: MERRA-2 dust mixing ratio at radiosonde deployment location and times along each AEROSER track, the shading indicates the dust mixing ratio as shown on the right.

useful for this study; aerosols in MERRA-2 are constrained via data assimilation, see Randles et al. (2017) and Buchard et al. (2017) for further details. Figure 2 (rows 5–6) shows the MERRA-2 dust mass mixing ratio at the radiosonde deployment location along with each AEROSER track; clearly, as intended, AEROSER campaigns have encountered significant Saharan dust outflows.

2.3. RRTMG

RRTMG (Iacono et al., 2008) was developed by Atmospheric and Environmental Research, Inc. and uses a correlated-k method to improve the computational efficiency of radiative transfer calculations by dividing

the longwave spectrum into 16 and shortwave spectrum into 14 continuous bands. The atmospheric relative humidity and air temperatures are from the radiosondes, the SST_{skin} and near surface air temperatures are those from M-AERI, the dust aerosol inputs are taken from the MERRA-2. The surface shortwave and longwave radiation are the outputs from RRTMG.

MERRA-2 provides the dust mixing ratio of each layer but RRTMG requires AOD as input; the 550 nm AOD for each layer in RRTMG can be expressed as:

$$\tau_{550nm} = \sum_{i=1}^{i=5} x_i \times b_{ext,i}(RH, 550nm) \times \delta z \quad (1)$$

MERRA-2 includes five different sizes of dust particles, where x_i is the dust aerosol mass mixing ratio of each size interval i with the effective dust radii of 0.64, 1.34, 2.32, 4.2, and 7.75 μm ; therefore dust is size-resolved into 5 size bins according to Tegen et al. (2004). The dust extinction coefficient is $b_{ext,i}$ and δz is the atmospheric layer thickness, RH is the relative humidity of the dust layer. The dust extinction coefficient, single-scattering albedo (SSA), and asymmetry factor vary as a function of the dust size and composition, and these parameters were taken from the lookup table of Randles et al. (2017). The dust aerosols were assumed to be well mixed within each layer of the modeled atmosphere; the overall extinction coefficients, SSAs, and asymmetry factors were calculated following Equations A1–A3 of Thorsen et al. (2020).

RRTMG longwave calculations require specifying the aerosol scattering properties at each of the 16 spectral bands; the Ångström exponent formula (Ångström, 1929) given in following Equation 2 was used to explicitly specify the spectral AOD, τ_λ , for a given wavelength λ in the radiative transfer calculations:

$$\frac{\tau_\lambda}{\tau_{550nm}} = \left(\frac{\lambda}{\lambda_{550nm}} \right)^{-\alpha} \quad (2)$$

where α is the aerosol Ångström exponent determined from the MERRA-2 Dust Angstrom parameter. MERRA-2 provides three-hourly averaged dust properties, so the dust profiles are linearly interpolated to the radiosonde deployment times and locations. Other inputs, such as the sea-surface emissivity and surface albedo are also taken from MERRA-2.

2.4. SST_{skin} Model

The Group for High Resolution Sea-Surface Temperature (GHRSSST) has defined different kinds of SSTs according to the depth and produced a suite of SST products (Donlon et al., 2007). Sea-Bird Thermosalinographs (TSG) were mounted near the ships' seawater intakes at a depth of 4.2 m on the NOAA S Ronald H. Brown and at 2.5 m on the R/V Alliance to measure the sea temperature that can approximate the foundation SST (SST_{fnd}) where the temperature is presumed to be free of diurnal variability.

There are many diurnal heating and cooling models with varying complexity and dependences on forcing parameters. Some models are driven by surface fluxes, such as those used in ERA-5 (Akella et al., 2017; ECMWF, 2016), and some others use ship measurements (Gentemann et al., 2009; Minnett et al., 2011; Zhang et al., 2020). The SST_{fnd} for this study is taken from the ship-based thermosalinographs. The SST_{skin} variations can be expressed by the cool skin layer and the warm layer schemes (Akella et al., 2017; ECMWF, 2016; Takaya et al., 2010; Zeng & Beljaars, 2005).

$$SST_{skin} = SST_{fnd} - \Delta SST_d + \Delta SST_w(z) \quad (3)$$

where SST_{fnd} , ΔSST_d and ΔSST_w are TSG SST_{fnd} , the vertical temperature difference across the cool-skin layer, and the temperature difference between the sub-skin and foundation temperatures, that is, the warm-skin layer. The ΔSST_d , can be expressed as:

$$\Delta SST_d = \frac{\delta}{\rho_w c_w k_w} (Q_c) \quad (4)$$

where ρ_w , k_w , c_w are the water density, thermal conductivity and volumetric heat capacity respectively, δ is the thermal skin layer thickness. Equation 4 is based on Saunders (1967) and developed by Fairall et al. (1996b) which includes the convections at the skin layer and the daytime shortwave insolation absorption. Q_c is the surface net heat flux in the cool-skin layer, which is positive downward:

$$Q_c = H_s + H_L - LW_{net} - f_s SW_{net} \quad (5)$$

where H_s , H_L , LW_{net} and SW_{net} are the sensible and latent heat flux, net longwave and solar radiation at the surface, but only a fraction, f_s , of the surface insolation is absorbed by the near surface ocean, given by Fairall et al. (1996a) and Fairall et al. (2003), f_s depends on the thickness of the skin layer, the wavelength of the absorbed solar radiation based on the results of Paulson and Simpson (1981), wind speed, and cleanness of the water (or type of the water). In this study we calculate that the f_s with Fairall et al., (1996a). Sensible and latent heat flux can be calculated by the updated version 3.6 Coupled Ocean–Atmosphere Response Experiment (COARE) algorithm (Fairall et al., 2003). The longwave and shortwave heat fluxes are from RRTMG output with and without aerosol.

The diurnal warming can be expressed as:

$$\frac{\partial(SST_{-\delta} - SST_{fnd})}{\partial t} = \frac{Q_w + R_s - R(-d)}{d\rho_w c_w \nu / (\nu + 1)} - \frac{(\nu + 1)k u_{*w} f(La)}{d\phi_t(d/L)} (SST_{-\delta} - SST_{fnd}) \quad (6)$$

where $SST_{-\delta}$ is the temperature at the base of the cool skin layer that is free of diurnal variability, d is the diurnal warming layer depth, ν is the profile shape due to the near-surface solar heating and wind conditions, having a value of 0.2 (Gentemann & Akella, 2018) in this study, u_{*w} is the water friction velocity and $u_{*w} = u_{*a} \sqrt{\rho_a / \rho_w}$; u_{*a} depends on the friction velocity in the atmosphere u_{*a} and the density of water (ρ_w) and air (ρ_a), κ is the von Karman constant of 0.4, $\phi_t(d/L)$ is the stability function discussed in the following Equation 8. La is the Langmuir number, $La = \sqrt{u_{*w}} / u_s$, Akella et al., [2017] parametrized the impact of Langmuir circulation. and $f(La) = La^{-2/3}$. The Stokes velocity, u_s , is taken as 0.01m/s, as by Akella et al. (2017). $R(-d)$ is the intensity of solar radiation at depth -d. Overall, the left hand side (LHS) represents the time-tendency of diurnal warming, first term on the RHS denotes heat input from surface and finally the second term on RHS denotes the dissipation due to wind (and in general turbulent mixing).

The stability parameter, d/L , includes the Obukhov length, L , given by

$$L = \frac{\rho_w c_w u_{*w}^3}{\kappa g \alpha_w Q_w} \quad (7)$$

The stability function $\phi_t(d/L)$ is:

$$\phi_t(d/L) = \begin{cases} 1 + \frac{5d/L + 4(d/L)^2}{1 + 3d/L + 0.25(d/L)^2} & \text{when } d/L \geq 0 \\ (1 - 16d/L)^{-0.5} & \text{when } d/L < 0 \end{cases} \quad (8)$$

The net heat flux, Q_w , available to heat the warming layer can be expressed as:

$$Q_w = SW_{net}^w + LW_{net} - H_s - H_L \quad (9)$$

Note the SW_{net}^w is the warming layer absorbed net shortwave radiation, $SW_{net}^w = SW_{net} - SW_{PEN}$, where SW_{PEN} is the penetrating short-wave radiation:

$$SW_{PEN} = SW_{net} \sum_{i=1}^{N=3} a_i \exp(-db_i) \quad (10)$$

the coefficients a_i and b_i can be obtained from Zeng and Beljaars (2005).

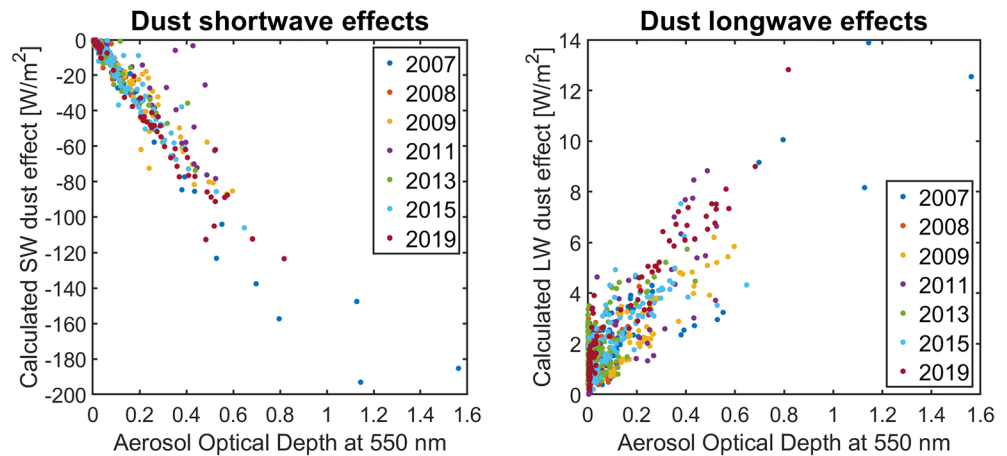


Figure 3. Left: RRTMG-calculated Saharan dust shortwave reduction at the sea surface with AOD at 550 nm at the radiosonde deployment stations. Right: RRTMG-calculated Saharan dust longwave increases. The colors indicate the year.

Integrating Equation 6 in time is part of the warm-skin layer scheme, the results of the warm layer and the cool layer schemes are added together (Equation 3) to derive the SST_{skin} . The net solar radiation at the surface SW_{net} and the net longwave radiation LW_{net} at the surface are taken from the RRTMG simulation outputs with and without aerosols (Section 3.1); so the SST_{skin} response to the dust can be expressed as the difference between the SST_{skin} schemes with and without aerosols.

3. Results and Discussion

3.1. Net Radiative Effects of Dust at the Sea Surface From RRTMG

The sea-surface heat budget is related to the shortwave and longwave net radiative heat fluxes and the turbulent latent and sensible fluxes at the surface. To quantify dust aerosol effects on the sea-surface heat budget and SST_{skin} , the downward shortwave and longwave radiation were estimated using radiative transfer calculations.

The downward irradiance is sensitive to the solar zenith angle, air temperature, water vapor, cloud and aerosol properties (Kato et al., 2018). Because directly measured SRF is available in only a limited area, the current global SRF data (Kato et al., 2018; Loeb et al., 2019, 2020) are calculated using radiative transfer models with input from satellite measurements and reanalysis fields. The AEROSE campaigns encountered significant Saharan dust outflow events as shown in Figure 2 (rows 5 and 6); and the measurements taken during the AEROSE campaigns provide basic inputs for atmospheric radiative transfer calculations in the tropical North Atlantic area.

RRTMG calculations with and without aerosols indicate the dust radiative effects on the SRF, which are defined here as the dust contaminated SRF minus the clear-sky SRF. Figure 3 shows the surface shortwave and longwave radiation changes due to the presence of dust aerosols.

Since the dust aerosols scatter and absorb the solar radiation that would otherwise reach the sea surface, there is a reduction in the surface shortwave radiation, as shown in Figure 3: Most of the negative anomalies are smaller than -90 W/m^2 , however, there are some extreme values from -120 W/m^2 to -190 W/m^2 for $\text{AOD} > 0.8$. Because most of the radiosondes were deployed shortly before AQUA satellite overpass times (around 13:30 ascending node time), the stronger solar insolation increases the calculated shortwave anomalies at these times to be above the diurnal-mean. The dust also emits longwave radiation which warms the sea surface; the dust aerosols introduced positive longwave flux anomalies as large as 14 W/m^2 in our simulations. Note that different (yearly) AEROSE campaigns would have encountered different vertical distribution of dust aerosols (shown in Figure 2), which could explain the differences among different years in Figure 3, for instance the much lower dust in 2013 (leg 2) leading to smaller shortwave radiation reduction.

Most of the large anomalies occurred during the AEROSE 2007 and 2019 cruises, because there were strong dust outbreaks during that time (Figure 2). Based on the RRTMG calculations, the dust aerosols introduce negative shortwave anomalies of $-130 \text{ W/m}^2/\text{AOD}$ and positive longwave anomalies of $12 \text{ W/m}^2/\text{AOD}$. Our calculated anomalies are significantly higher than other studies, for example Yu et al. (2006) found $-68 \text{ W/m}^2/\text{AOD}$ and Song et al. (2018) found $-83 \text{ W/m}^2/\text{AOD}$ direct radiative anomalies. This may be due to different model inputs, as other studies used satellite data as input, the abnormal atmospheric cases can introduce biases in the satellite-derived SRFs (Kato et al., 2020; Loeb et al., 2020). Also, our study is limited to outbreaks of Saharan dust aerosols in the North Atlantic area while other studies were based on larger research areas where there may be aerosols with different characteristics.

It is worth noting that for the RRTMG calculations, any inaccuracies in the MERRA-2 dust aerosols profiles, such as reported by Kramer et al. (2020), could introduce errors and uncertainties. MERRA-2 assimilates the AOD derived from satellite and in-situ measurements and determines the vertical distribution through the model physics. This study assumes that MERRA-2 provides reasonably accurate dust profiles; MERRA-2 AODs have been validated using independent dust aerosol observations from satellite, aircraft, and ground-based observations (Bosilovich et al., 2015; Buchard et al., 2017; Gelaro et al., 2017), the results show the AOD in MERRA-2 generally compared well.

3.2. SST_{skin} Response to Dust Radiative Effects

There have been several models [Gentemann et al., 2009; Minnett et al., 2011; Zhang & Zhang, 2012] that discuss the SST_{skin} variations as a function of wind speed: The SST_{skin} variation is weak under stronger wind and well-mixed conditions. As indicated by Foltz and McPhaden (2008), Lau and Kim (2007), Martínez Avellaneda et al. (2010), most of the cooling anomalies at our study regions are driven by surface wind stress, which modulates the sensible and latent heat loss and the horizontal current-introduced heat advection. The shortwave radiation anomalies do not produce as large an effect on SST_{skin} variability as wind stress; thus, only the situations with wind speed $<4\text{m/s}$ are selected here to reduce the wind stress forcing on SST_{skin} .

Figure 4 shows the time series of the SST_{skin} changes due to dust aerosol (top), and the distributions of the SST_{skin} change at the times and places of radiosonde launches (bottom). Clearly, the significant SST_{skin} changes are within the dust outflow region; overall, the dust aerosols introduce cooling anomalies to SST_{skin} . When the wind speed is low, the absorbed solar radiation leads to a stable stratification in the upper ocean that results in an increase in temperature located near the ocean surface, establishing a diurnal warming layer. The diurnal warming temperature increase can be several K, and it has been captured in field measurements (Donlon et al., 2002; Gentemann and Minnett, 2008; Minnett et al., 2011) and in satellite data (Gentemann et al., 2003; Marullo et al., 2010). However, the dust aerosols reduce the downward shortwave radiation, reducing the SST_{skin} by as much as -0.24 K . The overall cooling magnitudes are consistent with those of previous studies (Foltz & McPhaden, 2008).

The SST_{skin} response to dust-induced radiation changes for wind speed $<4\text{m/s}$ are plotted against AOD at 550 nm wavelength in Figure 5, separately by daytime (left) and nighttime (right). From the daytime linear regression analyses shown in Figure 5 (left), the AOD of 0.8–1.6 can introduce cooling effects as large as -0.24 K ; it can also introduce warming effects of 0.04 K during the daytime, depending on the solar zenith angle and dust layer's temperature and altitude. In general, when the solar zenith angle is small, the dust aerosols can block more downward shortwave radiation that reaches the Earth's surface and further decrease the SST_{skin} . However, when the solar zenith angle is $> 50^\circ$, the dust aerosol introduced surface shortwave anomalies may not be as large as the longwave anomalies; the increased downward longwave radiations can warm the sea surface. Thus, the dust aerosols can introduce both warm and cold anomalies to SST_{skin} during daytime, depending on the solar zenith angle. The results of studying different dust aerosol temperatures and altitudes will be reported in Section 4.

Since the SST is nearly everywhere higher than the air temperature, the upward longwave radiation is greater than downward. With the dust-introduced increased net longwave radiation (LW_{net} in Equation 5), the surface net heat flux Q_c will decrease, so the temperature drop across the thermal skin layer (ΔSST_d in Equation 3) will be reduced; thus the dust aerosol longwave radiation can introduce a warm SST_{skin} anomaly

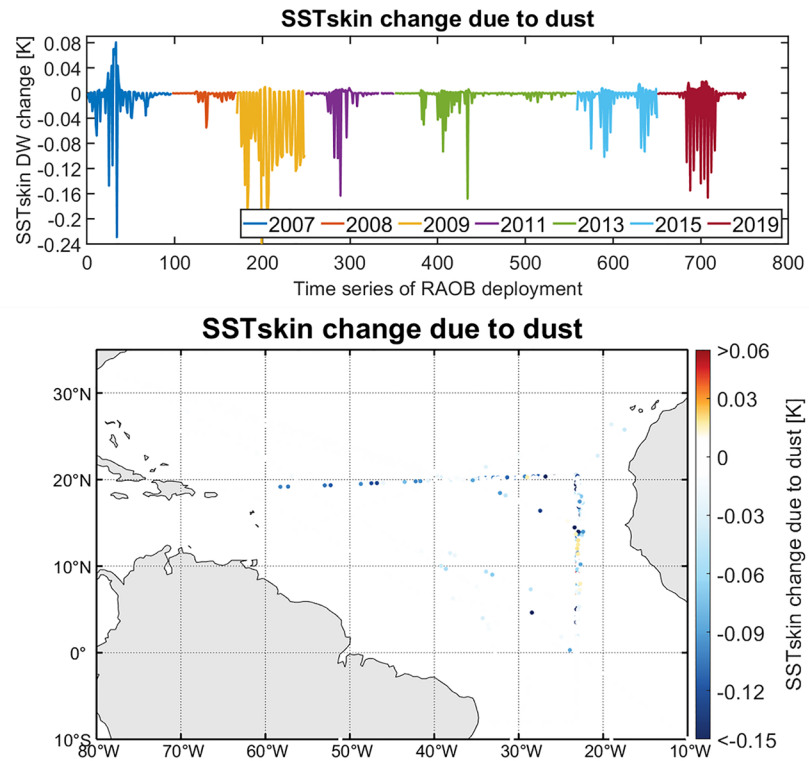


Figure 4. Top: Time series of the SST_{skin} changes due to dust. The x-axis is the radiosonde deployment number, and the y-axis shows the simulated SST_{skin} changes, which are calculated as the difference between the SST_{skin} with and without dust. The unit is K. The colors indicate the deployment year. Bottom: Geographic distributions of the calculated SST_{skin} changes due to dust. The colors indicate the SST_{skin} change due to dust, as shown on the right with the unit of K. Note there are many points which have almost zero SST_{skin} change. The latitude and longitude ranges are reduced compared to Figure 1.

during the nighttime, as shown in Figure 5 (right). However, the nighttime warming anomalies have only been calculated for low wind speeds; the averaged magnitudes of warming anomalies are usually < 0.03 K, and such a longwave heating anomaly by dust layer has usually been ignored in published studies. The dust-induced SST_{skin} anomalies are related to the AOD: There were strong dust outbreaks during 2007, 2009,

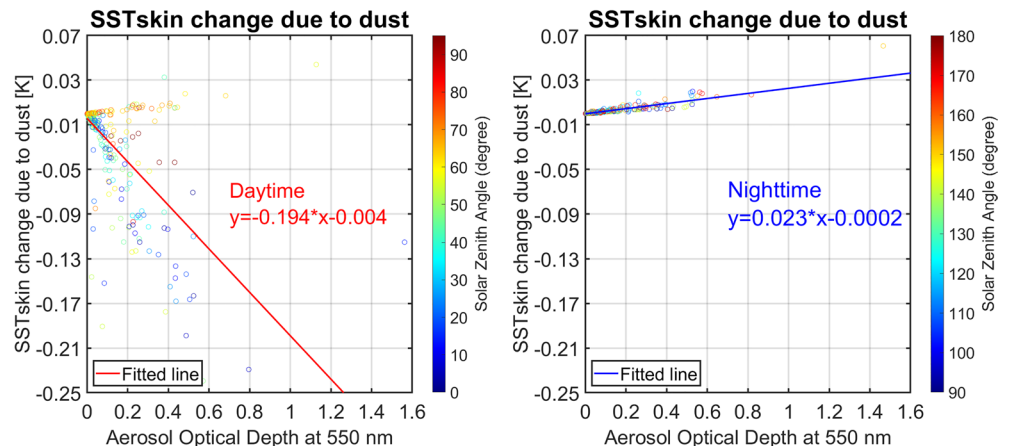


Figure 5. Left: Calculated daytime SST_{skin} changes due to dust with AOD at 550 nm, the SST_{skin} changes are large with high aerosol concentrations. Right: Calculated nighttime SST_{skin} changes.

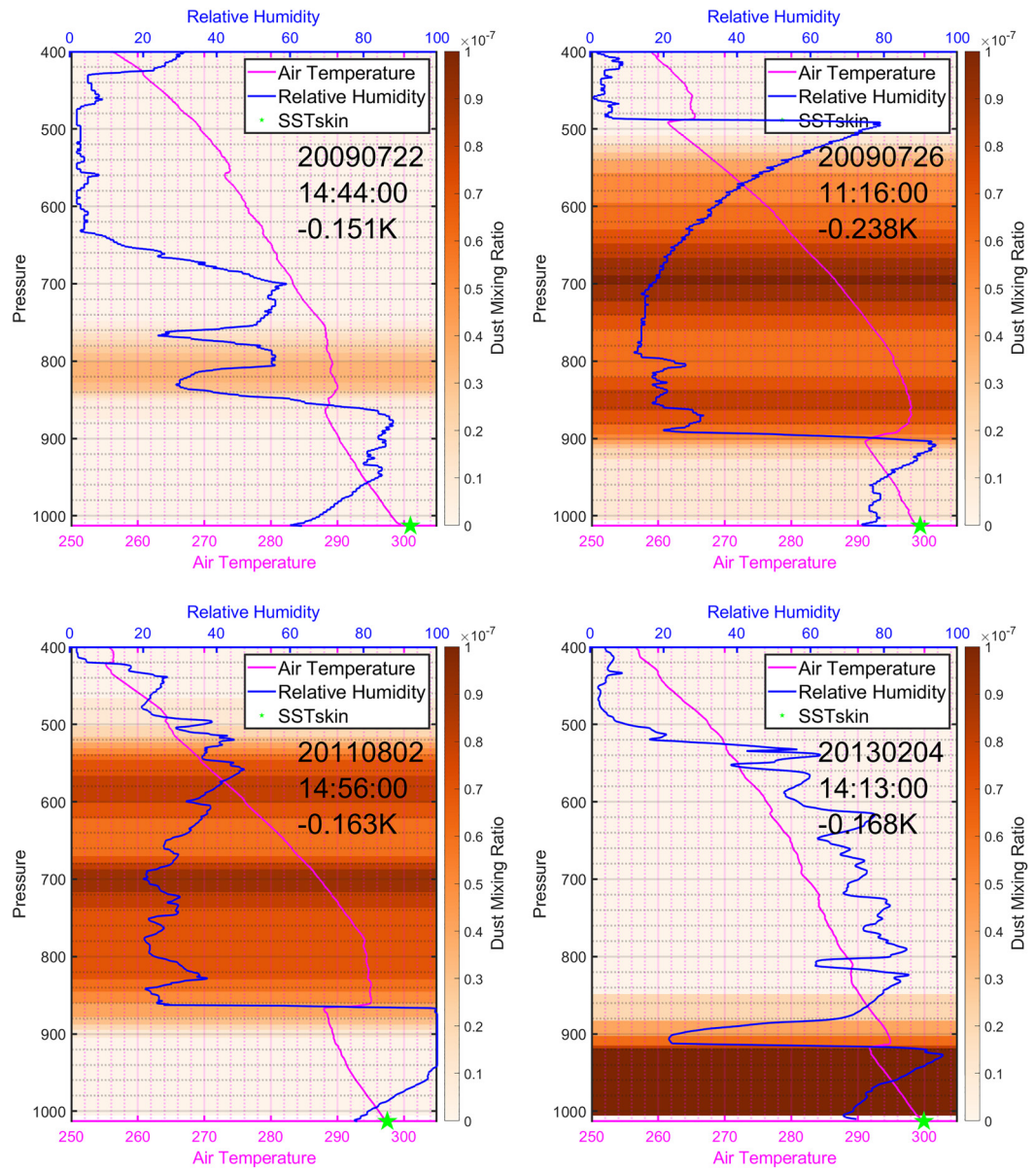


Figure 6. Atmospheric and SST_{skin} profiles when the dust aerosols reduce the SST_{skin} . Magenta and blue lines indicate relative humidity and air temperature profiles from radiosonde. Green star indicates the corresponding M-AERI measured SST_{skin} when radiosondes were deployed. The shading indicates the MERRA-2 DU002 dust mixing ratio as shown on the right with the unit of kg/kg.

and 2019 AEROSE cruises as shown in Figure 2 (rows 5–6); the corresponding SST_{skin} anomalies were larger during these years and near 15°N, 25°W, where the downward SRF had the greatest impact on SST_{skin} .

4. Cases of the Effects of Aerosol Variability

As discussed above, the downward SRF is modified by the dust aerosols. A comparison of individual radiosonde profiles with the MERRA-2 reanalyzed dust aerosol fields was made to assess the effects of dust layers encountered at different altitudes and with different vertical extents during the AEROSE cruises.

The AEROSE cruises sampled the Saharan dust outflow regions each year; the dust can be lifted to 400 hPa as shown in Figure 2 (rows 5 and 6). Figure 6 shows four situations when the dust aerosols reduce the SST_{skin} by -0.238 K to -0.151 K. The relative humidity and air temperature profiles measured by radiosondes are

plotted with blue and magenta lines; the M-AERI derived SST_{skin} is shown as the green star; the shading indicates the MERRA-2 DU002 dust mixing ratio as shown on color bar at right. The MERRA-2 dust mixing ratio during these four radiosonde deployments indicate large scale dust aerosol outflows; the elevated dust aerosol layers are always associated with dry air layers as shown in Figure 6. On July 22, 2009, 14:44 UTC, the dust aerosol layer was lifted to 800 hPa, but the dust concentration was not as large as in other situations shown; thus, the dust aerosols only reduced the SST_{skin} by -0.151K . On the days of July 26, 2009 and August 2, 2011, there were intense dust outbreaks extending vertically from 900 hPa to 500 hPa; the dust aerosols blocked large amounts of the downward shortwave radiation reaching the sea surface and further decrease the SST_{skin} by -0.238K and -0.163K respectively. The dust particles absorbed the shortwave radiation and warmed the lower troposphere, as shown by the temperature inversions at the bottom of the dust layer; the dry layers associated with the dust aerosol are also obvious. On February 4, 2013, the dust layer was not lifted to such high altitudes as on other days. The radiosonde captured the air temperature and relative humidity anomalies around 980 hPa associated with the aerosol dust layers. However, the dust layer temperatures were always lower than the SST_{skin} , which introduced a cold effect on the SST_{skin} .

Data from the AEROSE cruises provide a valuable way to test the dust effect on SST_{skin} under a variety of meteorological conditions. Figure 7 shows another four situations when the dust aerosols increase the SST_{skin} by $0.017\text{--}0.081\text{K}$. The two radiosonde profiles on May 14, 2007 show a warming effect when dust aerosol is present, and although the dust aerosols occur at high-altitude, to 650 hPa, the relatively high temperatures ($299\text{--}300\text{K}$ from 850hPa to 900hPa for dust layers) compared to the SST_{skin} lead to comparable warming effects. On the days when the ship *Ronald H. Brown* entered significant, large-scale warm dust outflow events, the warming SST_{skin} effects were more pronounced during nighttime or for large solar zenith angles. Similar situations can be seen on March 17, 2019, but the warming effects were not as large as during AEROSE 2007 when the dust layer temperature was higher than the SST_{skin} , the aerosol dust layers emitted radiation warmed the SST_{skin} .

The results from various radiosonde cases show the dust aerosol effect on SST_{skin} depends on several factors, such as the temperature contrast between the dust layer and SST_{skin} , the characteristics of the dust layer, concentration and altitude.

5. Summary

Previously published research has been directed at quantifying the direct dust effects on the SRF and SST using satellite data (e.g., Evan et al., 2009; Foltz & McPhaden 2008; Martínez Avellaneda et al., 2010; Song et al., 2018); however, the downward SRF derived from satellite measurements over the ocean have large uncertainties (Kato et al., 2018). Given the inaccuracies in satellite retrievals, accurate independent ship-board measurements in the tropical Atlantic Ocean area provide an independent representation of the atmosphere and ocean that can be used to investigate the influence of the dust aerosols on SST_{skin} variability. The NASA MERRA-2 reanalysis fields augment the radiosonde data to characterize the vertical dust aerosol profiles at the times and places where radiosondes were launched, and to provide inputs for radiative transfer calculations. This study includes the RRTMG-simulated surface shortwave and net longwave downwelling radiative changes due to dust and calculates the corresponding thermal skin layer temperature changes. The radiative transfer model was driven with oceanic and atmospheric variables taken from AEROSE cruises and from MERRA-2 fields resulting in estimates of radiative forcing of the SST_{skin} .

As our ship-based sampling covered weak to strong dust outbreaks, the dust aerosol effects on SST_{skin} also vary temporally and spatially. Based on the RRTMG model calculations under various dust distributions, we estimate the dust can introduce a reduction of up to 190W/m^2 in surface shortwave radiation at around 13:30 local time and an increase of 14W/m^2 surface longwave radiation. As the SST variability is mainly responsive to wind-induced turbulent latent and sensible heat loss at the surface (Foltz & McPhaden, 2008; Lau & Kim, 2007), we have simulated the SST_{skin} variations with models of the thermal skin layer for wind speeds $< 4\text{m/s}$. The dust aerosols can introduce warming and cooling anomalies to SST_{skin} during daytime, depending on the solar zenith angle, dust layer concentration, temperature and altitude; the reduction in surface shortwave radiation can decrease the SST_{skin} by as much as -0.24K . The anomalous increase in the surface longwave radiation is associated with an increase in SST_{skin} of up to 0.06K , which is identifiable at

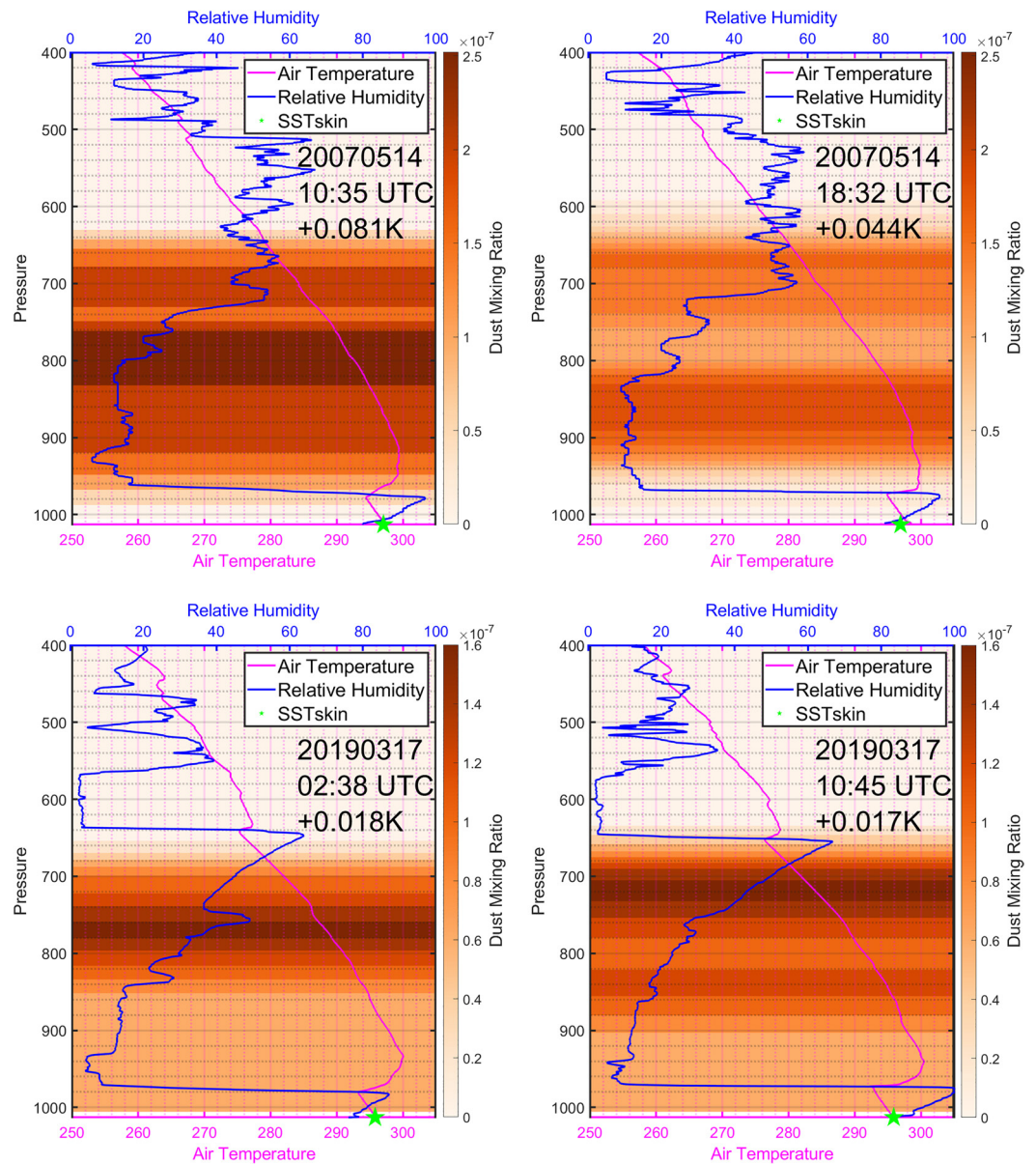


Figure 7. As Figure 6, but the dust aerosols increase the SST_{skin} .

daytime and nighttime. The cooling and warming anomalies cover a broad region with dust outbreaks and are strongest in the central sub-tropical North Atlantic Ocean, which are consistent with previous studies (Evan et al., 2011; Foltz & McPhaden, 2008).

This study combines in situ measurements with reanalysis fields to improve our knowledge of the dust forcing on SRF and SST_{skin} , which is key to understanding better the roles of aerosols and their feedbacks in the climate system. Reanalyzes such as MERRA-2, as they evolve into more comprehensive earth system reanalyzes, should include coupling feedbacks between ocean (via SST_{skin}), meteorology and aerosols. For instance, the satellite brightness temperatures that are assimilated in MERRA-2 and ERA-5 are mostly clear-sky radiances, that is, measurements that are deemed to be in cloudy, aerosol, or rain conditions are not assimilated in the infrared; ERA-5 includes “all-sky” microwave radiance data assimilation, see Hersbach et al. (2020) for details. Since reanalyzes (e.g., MERRA-2) capture detailed aerosol variability, how does that impact brightness temperature simulation? And in-turn, does that impact meteorological assimilation? The study of Kim et al. (2018) showed that indeed more accurate brightness temperatures can be simulated

by including aerosol information in radiative transfer modeling, however the computation cost was burdensome. A more recent work by Choi et al. (2020) also provide encouraging results in this direction. In closing we recommend that more detailed determination of the dust effects on SRF requires better knowledge of dust radiative properties and vertical profiles derived, for example, from ship-based lidar.

Data Availability Statement

M-AERI data are available through Minnett et al. (2020b); the NOAA Ship data along with PNE project can be found at <https://www.aoml.noaa.gov/phod/pne/cruises.php> and NOAA NCEI <https://data.noaa.gov/onestop/collections?q=ron%20brown>; the NASA MERRA-2 data is available through https://gmao.gsfc.nasa.gov/reanalysis/MERRA-2/data_access/. The at-sea support of the officers, crew, and colleagues of the NOAA Ship *Ronald H Brown* and R/V *Alliance* is appreciated.

Acknowledgments

This research was funded by NASA Physical Oceanography program (Grant # NNX14AK18G), and Future Investigators in NASA Earth and Space Science and Technology (FINESST) Program (Grant # 80NSSC19K1326). This work has benefited from discussions with colleagues at RSMAS. AEROSE is a collaboration with the NOAA PIRATA Northeast Extension (PNE) project and is supported by the NOAA Center for Atmospheric Sciences and Meteorology (NCAS-M) at Howard University, the New College for Interdisciplinary Arts and Sciences at Arizona State University (Prof. Vernon Morris, PI), the NOAA Educational Partnership Program grant NA17AE1625, NOAA grant NA17AE1623, the Joint Polar Satellite System (JPSS) and NOAA/NESDIS/STAR. SA was partially funded via NASA Modeling, Analysis and Prediction (MAP) program supported GMAO “core” funding, managed by Dr. David Considine (NASA HQ).

References

- Akella, S., Todling, R., & Suarez, M. (2017). Assimilation for skin SST in the NASA GEOS atmospheric data assimilation system. *Quarterly Journal of the Royal Meteorological Society*, *143*(703 Pt B), 1032–1046. <https://doi.org/10.1002/qj.2988>
- Ångström, A., & Ångström, A. (1929). On the atmospheric transmission of sun radiation and on dust in the air. *Geografiska Annaler*, *11*(2), 156–166. <https://doi.org/10.2307/519399>
- Bosilovich, M. G., et al. (2015). *MERRA-2: Initial evaluation of the climateRep.*, 145, NASA 426 Goddard Space Flight Center, Greenbelt, Maryland 20771, USA.
- Buchard, V., Randles, C. A., da Silva, A. M., Darmenov, A., Colarco, P. R., Govindaraju, R., et al. (2017). The MERRA-2 aerosol reanalysis, 1980 onward. Part II: Evaluation and case studies. *Journal of Climate*, *30*(17), 6851–6872. <https://doi.org/10.1175/jcli-d-16-0613.1>
- Carlson, T. N., & Prospero, J. M. (1972). The large-scale movement of Saharan air outbreaks over the northern equatorial Atlantic. *Journal of Applied Meteorology*, *11*(2), 283–297. [https://doi.org/10.1175/1520-0450\(1972\)011<0283:tmsos>2.0.co;2](https://doi.org/10.1175/1520-0450(1972)011<0283:tmsos>2.0.co;2)
- Choi, Y., Chen, S. H., Huang, C. C., Earl, K., Chen, C. Y., Schwartz, C. S., & Matsui, T. (2020). Evaluating the impact of assimilating aerosol optical depth observations on dust forecasts over North Africa and the East Atlantic using different data assimilation methods. *Journal of Advances in Modeling Earth Systems*, *12*(4), e2019MS001890. <https://doi.org/10.1029/2019MS001890>
- Doherty, O. M., & Evan, A. T. (2014). Identification of a new dust-stratocumulus indirect effect over the tropical North Atlantic. *Geophysical Research Letters*, *41*(19), 6935–6942. <https://doi.org/10.1002/2014gl060897>
- Donlon, C., Robinson, I., Casey, K. S., Vazquez-Cuervo, J., Armstrong, E., Arino, O., et al. (2007). The global ocean data assimilation experiment high-resolution sea surface temperature pilot project. *Bulletin of the American Meteorological Society*, *88*(8), 1197–1214. <https://doi.org/10.1175/bams-88-8-1197>
- Donlon, C. J., Martin, M., Stark, J., Roberts-Jones, J., Fiedler, E., & Wimmer, W. (2012). The Operational Sea Surface Temperature and Sea Ice Analysis (OSTIA) system. *Remote Sensing of Environment*, *116*(0), 140–158. <https://doi.org/10.1016/j.rse.2010.10.017>
- Donlon, C. J., Minnett, P. J., Gentemann, C., Nightingale, T. J., Barton, I. J., Ward, B., & Murray, M. J. (2002). Toward improved validation of satellite sea surface skin temperature measurements for climate research. *Journal of Climate*, *15*(4), 353–369.
- Union, J. P., & Velden, C. S. (2004). The impact of the Saharan air layer on Atlantic tropical cyclone activity. *Bulletin of the American Meteorological Society*, *85*(3), 353–366. <https://doi.org/10.1175/bams-85-3-353>
- ECMWF. (2016). Part IV: Physical Processes. In *IFS documentation CY43R1*. ECMWF. Retrieved from <https://www.ecmwf.int/en/elibrary/17117-ifs-documentation-cy43r1-part-iv-physical-processes>
- Evan, A. T., Foltz, G. R., Zhang, D., & Vimont, D. J. (2011). Influence of African dust on ocean-atmosphere variability in the tropical Atlantic. *Nature Geoscience*, *4*(11), 762–765. <https://doi.org/10.1038/ngeo1276>
- Evan, A. T., Vimont, D. J., Heidegger, A. K., Kossin, J. P., & Bennartz, R. (2009). The role of aerosols in the evolution of tropical North Atlantic Ocean temperature anomalies. *Science*, *324*(5928), 778. <https://doi.org/10.1126/science.1167404>
- Fairall, C. W., Bradley, E. F., Godfrey, J. S., Wick, G. A., Edson, J. B., & Young, G. S. (1996a). Cool-skin and warm-layer effects on sea surface temperature. *Journal of Geophysical Research*, *101*(C1), 1295–1308. <https://doi.org/10.1029/95jc03190>
- Fairall, C. W., Bradley, E. F., Hare, J. E., Grachev, A. A., & Edson, J. B. (2003). Bulk parameterization of air-sea fluxes: Updates and verification for the COARE algorithm. *Journal of Climate*, *16*(4), 571–591. [https://doi.org/10.1175/1520-0442\(2003\)016<0571:bpoasf>2.0.co;2](https://doi.org/10.1175/1520-0442(2003)016<0571:bpoasf>2.0.co;2)
- Fairall, C. W., Bradley, E. F., Rogers, D. P., Edson, J. B., & Young, G. S. (1996b). Bulk parameterization of air-sea fluxes for tropical ocean-global atmosphere coupled-ocean atmosphere response experiment. *Journal of Geophysical Research*, *101*(C2), 3747–3764. <https://doi.org/10.1029/95jc03205>
- Foltz, G. R., & McPhaden, M. J. (2008). Impact of saharan dust on tropical North Atlantic SST. *Journal of Climate*, *21*(19), 5048–5060. <https://doi.org/10.1175/2008jcli2232.1>
- Gelaro, R., McCarty, W., Suárez, M. J., Todling, R., Molod, A., Takacs, L., et al. (2017). The Modern-Era Retrospective Analysis for Research and Applications, Version 2 (MERRA-2). *Journal of Climate*, *30*(13), 5419–5454. <https://doi.org/10.1175/jcli-d-16-0758.1>
- Gentemann, C. L., & Akella, S. (2018). Evaluation of NASA GEOS-ADAS modeled diurnal warming through comparisons to SEVIRI and AMSR2 SST observations. *Journal of Geophysical Research Oceans*, *123*(2), 1364–1375. <https://doi.org/10.1002/2017JC013186>
- Gentemann, C. L., Donlon, C. J., Stuart-Menteth, A., & Wentz, F. J. (2003). Diurnal signals in satellite sea surface temperature measurements. *Geophysical Research Letters*, *30*(3), 1140–1143. <https://doi.org/10.1029/2002gl016291>
- Gentemann, C. L., & Minnett, P. J. (2008). Radiometric measurements of ocean surface thermal variability. *Journal of Geophysical Research*, *113*(C8), C08017. <https://doi.org/10.1029/2007JC004540>
- Gentemann, C. L., Minnett, P. J., & Ward, B. (2009). Profiles of Ocean Surface Heating (POSH): A new model of upper ocean diurnal warming. *Journal of Geophysical Research*, *114*(C7), C07017. <https://doi.org/10.1029/2008JC004825>
- Hansell, R. A., Tsay, S. C., Ji, Q., Hsu, N. C., Jeong, M. J., Wang, S. H., et al. (2010). An assessment of the surface longwave direct radiative effect of airborne Saharan dust during the NAMMA field campaign. *Journal of the Atmospheric Sciences*, *67*(4), 1048–1065. <https://doi.org/10.1175/2009jas3257.1>

- Hersbach, H., et al. (2020). The ERA5 global reanalysis. *Quarterly Journal of the Royal Meteorological Society*, (1–51). <https://doi.org/10.1002/qj.3803>
- Iacono, M. J., Delamere, J. S., Mlawer, E. J., Shephard, M. W., Clough, S. A., & Collins, W. D. (2008). Radiative forcing by long-lived greenhouse gases: Calculations with the AER radiative transfer models. *Journal of Geophysical Research*, 113(D13). <https://doi.org/10.1029/2008jd009944>
- Kato, S., Loeb, N. G., Rose, F. G., Doelling, D. R., Rutan, D. A., Caldwell, T. E., et al. (2013). Surface irradiances consistent with CERES-derived top-of-atmosphere shortwave and longwave irradiances. *Journal of Climate*, 26(9), 2719–2740. <https://doi.org/10.1175/jcli-d-12-00436.1>
- Kato, S., Rose, F. G., Rutan, D. A., Thorsen, T. J., Loeb, N. G., Doelling, D. R., et al. (2018). Surface irradiances of edition 4.0 Clouds and the Earth's Radiant Energy System (CERES) Energy Balanced and Filled (EBAF) Data Product. *Journal of Climate*, 31(11), 4501–4527. <https://doi.org/10.1175/jcli-d-17-0523.1>
- Kato, S., Rutan, D. A., Rose, F. G., Caldwell, T. E., Ham, S.-H., Radkevich, A., et al. (2020). Uncertainty in satellite-derived surface irradiances and challenges in producing surface radiation budget climate data record. *Remote Sensing*, 12(12), 1950. <https://doi.org/10.3390/rs12121950>
- Kearns, E. J., Hanafin, J. A., Evans, R. H., Minnett, P. J., & Brown, O. B. (2000). An independent assessment of pathfinder AVHRR sea surface temperature accuracy using the Marine Atmosphere Emitted Radiance Interferometer (MAERI). *Bulletin of the American Meteorological Society*, 81(7), 1525–1536. [https://doi.org/10.1175/1520-0477\(2000\)081<1525:aiaopa>2.3.co;2](https://doi.org/10.1175/1520-0477(2000)081<1525:aiaopa>2.3.co;2)
- Kilpatrick, K. A., Podestá, G., Walsh, S., Williams, E., Halliwell, V., Szczodrak, M., et al. (2015). A decade of sea surface temperature from MODIS. *Remote Sensing of Environment*, 165, 27–41. <https://doi.org/10.1016/j.rse.2015.04.023>
- Kim, J., Akella, S., da Silva, A. M., Todling, R., & McCarty, W. (2018). Preliminary evaluation of influence of aerosols on the simulation of brightness temperature in the NASA's goddard earth observing system atmospheric data assimilation system. *NASA Technical Report Series on Global Modeling and Data Assimilation*, 49. Retrieved from <https://ntrs.nasa.gov/archive/nasa/casi.ntrs.nasa.gov/20180001946.pdf>
- Kok, J. F., Ridley, D. A., Zhou, Q., Miller, R. L., Zhao, C., Heald, C. L., et al. (2017). Smaller desert dust cooling effect estimated from analysis of dust size and abundance. *Nature Geoscience*, 10(4), 274–278. <https://doi.org/10.1038/ngeo2912>
- Kramer, S. J., Alvarez, C., Barkley, A. E., Colarco, P. R., Custals, L., Delgado, R., et al. (2020). Apparent dust size discrepancy in aerosol reanalysis in north African dust after long-range transport. *Atmospheric Chemistry and Physics*, 20(16), 10047–10062. <https://doi.org/10.5194/acp-20-10047-2020>
- Lau, K. M., & Kim, K. M. (2007). Cooling of the atlantic by saharan dust. *Geophysical Research Letters*, 34(23), L23811. <https://doi.org/10.1029/2007GL031538>
- Loeb, N. G., Rose, F. G., Kato, S., Rutan, D. A., Su, W., Wang, H., et al. (2020). Toward a consistent definition between satellite and model clear-sky radiative fluxes. *Journal of Climate*, 33(1), 61–75. <https://doi.org/10.1175/jcli-d-19-0381.1>
- Loeb, N. G., Wang, H., Rose, F. G., Kato, S., Smith, W. L., Jr., & Sun-Mack, S. (2019). Decomposing shortwave top-of-atmosphere and surface radiative flux variations in terms of surface and atmospheric contributions. *Journal of Climate*, 32(16), 5003–5019. <https://doi.org/10.1175/jcli-d-18-0826.1>
- Luo, B., & Minnett, P. J. (2020). Evaluation of the ERA5 sea surface skin temperature with remotely-sensed shipborne marine-atmospheric emitted radiance interferometer data. *Remote Sensing*, 12(11), 1873. <https://doi.org/10.3390/rs12111873>
- Luo, B., & Minnett, P. J. (2021). Skin sea surface temperatures from the GOES-16 ABI validated with those of the shipborne M-AERI. *IEEE Transactions on Geoscience and Remote Sensing*, 1–12. <https://doi.org/10.1109/TGRS.2021.3054895>
- Luo, B., Minnett, P. J., Gentemann, C., & Szczodrak, G. (2019). Improving satellite retrieved night-time infrared sea surface temperatures in aerosol contaminated regions. *Remote Sensing of Environment*, 223, 8–20. <https://doi.org/10.1016/j.rse.2019.01.009>
- Luo, B., Minnett, P. J., & Nalli, N. R. (2021). Infrared satellite-derived sea surface skin temperature sensitivity to aerosol vertical distribution—Field data analysis and model simulations. *Remote Sensing of Environment*, 252, 112151. <https://doi.org/10.1016/j.rse.2020.112151>
- Luo, B., Minnett, P. J., Szczodrak, M., Kilpatrick, K., & Izaguirre, M. (2020a). Validation of Sentinel-3A SLSTR derived sea-surface skin temperatures with those of the shipborne M-AERI. *Remote Sensing of Environment*, 244, 111826. <https://doi.org/10.1016/j.rse.2020.111826>
- Luo, B., Minnett, P. J., Szczodrak, M., Nalli, N. R., & Morris, V. R. (2020b). Accuracy assessment of MERRA-2 and ERA-Interim sea surface temperature, air temperature, and humidity profiles over the Atlantic Ocean using AEROSÉ measurements. *Journal of Climate*, 33(16), 6889–6909. <https://doi.org/10.1175/JCLI-D-19-0955.1>
- Martínez Avellaneda, N., Serra, N., Minnett, P. J., & Stammer, D. (2010). Response of the eastern subtropical Atlantic SST to Saharan dust: A modeling and observational study. *Journal of Geophysical Research*, 115(C8). <https://doi.org/10.1029/2009jc005692>
- Marullo, S., Santoleri, R., Banzon, V., Evans, R. H., & Guarracino, M. (2010). A diurnal-cycle resolving sea surface temperature product for the tropical Atlantic. *Journal of Geophysical Research*, 115(C5), C05011. <https://doi.org/10.1029/2009JC005466>
- Merchant, C. J., Embury, O., Le Borgne, P., & Bellec, B. (2006). Saharan dust in nighttime thermal imagery: Detection and reduction of related biases in retrieved sea surface temperature. *Remote Sensing of Environment*, 104(1), 15–30. <https://doi.org/10.1016/j.rse.2006.03.007>
- Minnett, P. J., Kilpatrick, K. A., Podestá, G. P., Evans, R. H., Szczodrak, M. D., Izaguirre, M. A., et al. (2020a). Skin Sea-Surface Temperature from VIIRS on Suomi-NPP-NASA Continuity Retrievals. *Remote Sensing*, 12(20), 3369. <https://doi.org/10.3390/rs12203369>
- Minnett, P. J., Knuteson, R. O., Best, F. A., Osborne, B. J., Hanafin, J. A., & Brown, O. B. (2001). The marine-atmospheric emitted radiance interferometer: A high-accuracy, seagoing infrared spectroradiometer. *Journal of Atmospheric and Oceanic Technology*, 18(6), 994–1013. [https://doi.org/10.1175/1520-0426\(2001\)018%3C0994:TMAERI%3E2.0.CO;2](https://doi.org/10.1175/1520-0426(2001)018%3C0994:TMAERI%3E2.0.CO;2)
- Minnett, P. J., Smith, M., & Ward, B. (2011). Measurements of the oceanic thermal skin effect. *Deep Sea Research Part II: Topical Studies in Oceanography*, 58(6), 861–868. <https://doi.org/10.1016/j.dsr2.2010.10.024>
- Minnett, P. J., Szczodrak, M. D., Izaguirre, M. A., & Luo, B. (2020b). Ship-based high resolution sea surface skin temperature from the Marine-Atmospheric Emitted Radiance Interferometer (M-AERI) deployed between 2013 and 2020 University of Miami. <https://doi.org/10.17604/bswq-0119>
- Morris, V., Clemente-Colón, P., Nalli, N. R., Joseph, E., Armstrong, R. A., Detrés, Y., et al. (2006). Measuring trans-atlantic aerosol transport from africa. *EOS. Transactions - American Geophysical Union*, 87(50), 565–571. <https://doi.org/10.1029/2006eo500001>
- Nalli, N. R., Joseph, E., Morris, V. R., Barnet, C. D., Wolf, W. W., Wolfe, D., et al. (2011). Multiyear observations of the tropical Atlantic atmosphere: Multidisciplinary applications of the NOAA aerosols and ocean science expeditions. *Bulletin of the American Meteorological Society*, 92(6), 765–789. <https://doi.org/10.1175/2011BAMS2997.1>
- Paulson, C. A., & Simpson, J. J. (1981). The temperature difference across the cool skin of the ocean. *Journal of Geophysical Research*, 86(C11), 11044–11054. <https://doi.org/10.1029/JC086iC11p11044>

- Randles, C. A., Da Silva, A. M., Buchard, V., Colarco, P. R., Darmenov, A., Govindaraju, R., et al. (2017). The MERRA-2 aerosol reanalysis, 1980 - onward, Part I: System description and data assimilation evaluation. *Journal of Climate*, *30*(17), 6823–6850. <https://doi.org/10.1175/JCLI-D-16-0609.1>
- Reynolds, R. W., & Smith, T. M. (1994). Improved Global Sea Surface Temperature Analyses Using Optimum Interpolation. *Journal of Climate*, *7*(6), 929–948. [https://doi.org/10.1175/1520-0442\(1994\)007<0929:igssta>2.0.co;2](https://doi.org/10.1175/1520-0442(1994)007<0929:igssta>2.0.co;2)
- Saunders, P. M. (1967). The temperature at the ocean-air interface. *Journal of the Atmospheric Sciences*, *24*(3), 269–273. [https://doi.org/10.1175/1520-0469\(1967\)024<0269:ttatoa>2.0.co;2](https://doi.org/10.1175/1520-0469(1967)024<0269:ttatoa>2.0.co;2)
- Song, Q., Zhang, Z., Yu, H., Seiji, K., Yang, P., Colarco, P., et al. (2018). Net radiative effects of dust in the tropical North Atlantic based on integrated satellite observations and in situ measurements. *Atmospheric Chemistry and Physics*, *18*, 11303–11322. <https://doi.org/10.5194/acp-18-11303-2018>
- Szczodrak, M., Minnett, P. J., Nalli, N. R., & Feltz, W. F. (2007). Profiling the lower troposphere over the ocean with infrared hyperspectral measurements of the marine-atmosphere emitted radiance interferometer. *Journal of Oceanic and Atmospheric Technology*, *24*(3), 390–402. <https://doi.org/10.1175/jtech1961.1>
- Takaya, Y., Bidlot, J.-R., Beljaars, A. C. M., & Janssen, P. A. E. M. (2010). Refinements to a prognostic scheme of skin sea surface temperature. *Journal of Geophysical Research*, *115*(C6). <https://doi.org/10.1029/2009JC005985>
- Tegen, I., Werner, M., Harrison, S. P., & Kohfeld, K. E. (2004). Relative importance of climate and land use in determining present and future global soil dust emission. *Geophysical Research Letters*, *31*(5). <https://doi.org/10.1029/2003gl019216>
- Thorsen, T. J., Ferrare, R. A., Kato, S., & Winker, D. M. (2020). Aerosol direct radiative effect sensitivity analysis. *Journal of Climate*, *33*(14), 6119–6139. <https://doi.org/10.1175/jcli-d-19-0669.1>
- Vimont, D. J., & Kossin, J. P. (2007). The Atlantic meridional mode and hurricane activity. *Geophysical Research Letters*, *34*(7). <https://doi.org/10.1029/2007gl029683>
- Wild, M., Folini, D., Schär, C., Loeb, N., Dutton, E. G., & König-Langlo, G. (2013). The global energy balance from a surface perspective. *Climate Dynamics*, *40*(11–12), 3107–3134. <https://doi.org/10.1007/s00382-012-1569-8>
- Wu, L. (2007). Impact of Saharan air layer on hurricane peak intensity. *Geophysical Research Letters*, *34*(9). <https://doi.org/10.1029/2007gl029564>
- Yamada, K., & Hayasaka, T. (2016). Evaluation of the accuracy of downward radiative flux observations at the sea surface. *Journal of Oceanography*, *72*(4), 553–565. <https://doi.org/10.1007/s10872-015-0345-x>
- Yu, H., Kaufman, Y. J., Chin, M., Feingold, G., Remer, L. A., Anderson, T. L., et al. (2006). A review of measurement-based assessments of the aerosol direct radiative effect and forcing. *Atmospheric Chemistry and Physics*, *6*(3), 613–666. <https://doi.org/10.5194/acp-6-613-2006>
- Zeng, X., and A. Beljaars, (2005). A prognostic scheme of sea surface skin temperature for modeling and data assimilation. *Geophysical Research Letters*, *32*(14), L14605. <https://doi.org/10.1029/2005GL023030>
- Zhang, H., Beggs, H., Ignatov, A., & Babanin, A. V. (2020). Nighttime cool skin effect observed from Infrared SST Autonomous Radiometer (ISAR) and depth temperatures. *Journal of Atmospheric and Oceanic Technology*, *37*(1), 33–46. <https://doi.org/10.1175/jtech-d-19-0161.1>
- Zhang, H., McFarquhar, G. M., Saleeby, S. M., & Cotton, W. R. (2007). Impacts of Saharan dust as CCN on the evolution of an idealized tropical cyclone. *Geophysical Research Letters*, *34*(14). <https://doi.org/10.1029/2007gl029876>
- Zhang, Y., & Zhang, X. (2012). Ocean haline skin layer and turbulent surface convections. *Journal of Geophysical Research*, *117*(C4), C04017. <https://doi.org/10.1029/2011JC007464>
- Zuidema, P., Xue, H., & Feingold, G. (2008). Shortwave radiative impacts from aerosol effects on marine shallow cumuli. *Journal of the Atmospheric Sciences*, *65*(6), 1979–1990. <https://doi.org/10.1175/2007jas2447.1>